Materials and Structures
DOI 10.1617/s11527-010-9634-4

ORIGINAL ARTICLE

Strain rate dependence of HPFRCC cylinders in monotonic tension

K. S. Douglas · S. L. Billington

Received: 2 June 2009 / Accepted: 13 June 2010

Abstract High-Performance Fiber-Reinforced Cementitious Composite (HPFRCC) materials exhibit strain hardening in uniaxial, monotonic tension accompanied by multiple cracking. The durability of HPFRCC materials under repeated loading makes them potentially suitable for seismic design applications. In this paper, the strain rate dependence of tensile properties of two HPFRCC materials in cylindrical specimens is reported from a larger study on strain rate effects in tension, compression and cyclic tension–compression loading. The cylindrical specimens were loaded in monotonic tension at strain rates ranging from quasi-static to 0.2 s^{-1}. To evaluate the impact of specimen geometry on tensile response, coupon specimens loaded in monotonic tension under a quasi-static strain rate were compared to corresponding cylindrical specimens made from the same batch of material. Tensile strength and ductility of the HPFRCC materials were significantly reduced with increasing strain rate. Multiple cracking, strain hardening, strain capacity, and the shape of the stress–strain response were found to be dependent on specimen geometry. SEM images taken of the fracture plane of several specimens indicated that pullout and fracture of the fibers occurred for both HPFRCC materials studied here.

Keywords Fiber-reinforced · Ductile cementitious composites · Strain rate · Tension testing

K. S. Douglas
CalStar Products, Inc., Newark, CA, USA

S. L. Billington (✉)
Stanford University, Stanford, CA, USA
e-mail: billington@stanford.edu

Published online: 06 July 2010

1 Introduction

High-Performance Fiber-Reinforced Cementitious Composite (HPFRCC) materials are a class of fiber-reinforced materials that exhibit strain hardening in uniaxial, monotonic tension accompanied by multiple cracking [22]. The strain hardening and multiple cracking behavior of HPFRCC materials leads to tensile strain capacities of 0.5–5%, depending on the material and specimen geometry. The primary distinction between HPFRCC and FRC materials is the ability to strain-harden and exhibit multiple cracking with a relatively low volume fraction (less than 2%) of fibers. The large tensile strain capacity of these materials allows for a relatively large energy absorption capacity. For this reason, HPFRCC materials are being heavily investigated for their use in seismic applications (overviews in Billington [1], Li [13], Parra-Montesinos [24], amongst others).

Simulation methods are needed to predict accurately the impact of using these materials in large structures subjected to seismic loads. However, it is not known if current constitutive models for HPFRCC (e.g., [7]) must be modified to account for elevated

strain rate response. Limited research has been conducted on the rate dependence of hybrid and single-fiber HPFRCCs in monotonic tension as discussed in Sect. 2.

The effect of strain rate on the tensile, compressive, and cyclic properties of HPFRCC materials was investigated [5] and the results of the strain rate dependence of tensile properties of two HPFRCC materials investigated are presented here. Cylindrical specimens were selected for investigation both because of their potential ability to represent bulk properties of HPFRCC cast in large elements and for consistency with the larger study on compression and cyclic tension–compression response, where cylindrical specimens were required. To assess the results relative to the majority of tensile studies of HPFRCC materials, which are conducted with thin coupon or dogbone specimens, a small geometry study was also conducted and is reported herein.

2 Background on HPFRCC materials investigated

The two HPFRCC materials studied were Engineered Cementitious Composites (ECC), which uses polymeric fibers (polyvinyl alcohol, PVA) with a coating specific for ECC in a mortar matrix, and an HPFRCC material consisting of high-strength, twisted steel fibers, also in a mortar matrix.

ECC is designed to exhibit steady-state cracking in uniaxial tension [14], resulting in the formation of multiple, very fine cracks (less than 100 μm). During the strain-hardening phase of loading, stress transfer from the fibers to the matrix is through interfacial shear alone and the fibers debond from the matrix. If the fibers cannot debond, then they will rupture, limiting the strain capacity of the composite. Maalej et al. [17] investigated uniaxial tensile strain rate effects in hybrid-fiber ECC (i.e., steel and polyethylene fibers). Tensile strength was reported to double as the strain rate increased from 2×10^{-6} to 2×10^{-1} s^{-1}, and multiple cracking, strain hardening and strain capacity were not affected. Yang and Li [34] reported similar tensile strength increases for ECC using PVA fibers alone and loaded at strain rates from 10^{-5} to 10^{-1} s^{-1}. Tensile strain capacity was reported to have decreased significantly due to the fiber interfacial chemical bond strength.

The second material investigated was a steel-fiber HPFRCC, wherein strain hardening and ductility are achieved by increasing the bond strength through frictional resistance and mechanical anchorage of the steel fibers during pullout. The steel fibers used have a polygonal cross section and are twisted along their longitudinal axis to give the fiber a helical shape. During pullout, which generally occurs after first cracking, the fibers tend to straighten, creating additional resistance to pullout at relatively large loads for slips as high as 70–80% of the initial embedded length [20, 28]. While adhesion between the fibers and the matrix is typically small, it has been shown during dynamic pullout tests that bond strength and bond stiffness both increase with crack displacement rate for flat-ended steel fibers [21]. The rate-sensitivity of high-strength, steel-fiber HPFRCC materials in tension was examined by Kim et al. [11] using strain rates of 10^{-4} to 10^{-1} s^{-1}. Dynamic increase factors up to 2.0 and 1.7 were observed for the first-cracking strength and post-cracking strength, respectively, depending on fiber type, fiber volume fraction, and matrix strength. Strain capacity remained largely unaffected by strain rate. The rate sensitivity of twisted steel fibers during pullout tests was attributed to radial and longitudinal cracking at the fiber-matrix interface that occurs as the fibers untwist during pullout. This rate sensitivity in fiber pullout, however, did not lead to increased rate dependence in composites with higher volume fractions.

Previous research on rate-dependence in ECC materials under uniaxial tension has been conducted on thin (e.g., 12–25 mm) coupon specimens. Likewise for twisted, steel fiber HPFRCC studies, testing has been carried out on thin (e.g., 25 mm) dogbone specimens. The previously studied, thin specimens are generally cast horizontally, which facilitates fiber alignment in the direction of loading, and this alignment may not be present in the materials when cast in bulk for structural applications. Here, cylindrical specimens, cast vertically and having a diameter of 50 mm (1.6–4 times the length of the fibers used) are investigated. In addition to the cylindrical shape potentially being more representative of bulk HPFRCC properties, it also facilitated consistent specimen geometry in the larger testing program involving compression and cyclic tension–compression testing [4, 5].

3 Experimental program

In this research, HPFRCC materials and one mortar were tested in monotonic tension at four strain rates ranging from quasi-static to seismic-level (total of 32 specimens). The rate sensitivity of these materials in tension was evaluated in terms of their first cracking strength, post-cracking strength, and strain capacity. Specific interest was paid to the strain capacity since it is this property of HPFRCC materials that permits energy absorption and makes them attractive to seismic applications. In addition, a geometry study was conducted in collaboration with researchers at the University of Michigan (total of eight specimens) to investigate the effects of specimen geometry on strain capacity, and to observe differences in response when the HPFRCC material was manufactured in different laboratories.

3.1 Materials and fabrication

Three HPFRCC mix designs (Table 1) and one reference mortar mix were evaluated to study the effects of strain rate on the tensile response of HPFRCC materials. Two HPFRCC mixtures were ECC materials with a 2% volume fraction of short, randomly distributed, high-modulus PVA fibers (Table 2). The ECC mix contains fine silica sand with an average particle diameter less than 0.2 mm. The ECC mix design used for the strain rate experiments, HP-E1, was repeated twice to test reproducibility, with the first set of experiments labeled as HP-E1A and the second set as HP-E1B. The ECC mix design used for the specimen geometry study is referred to as HP-E2. Note that the mix designs for HP-E1 and HP-E2 differ significantly in the amount of fly ash, w/cm ratio, and superplasticizer content. Additionally, HP-E1 contains methylcellulose which helps prevent the fibers from settling during mixing and casting. No direct comparisons across HP-E1 and HP-E2 will be made.

The steel-fiber HPFRCC mix, HP-T1, was reinforced with a 2% volume fraction of 30-mm long steel fibers (Tables 1 and 2). The fibers have a triangular cross section (equivalent diameter of 0.3 mm) and are twisted along their longitudinal axis. Flint silica sand with a maximum particle diameter of 0.6 mm was used. In addition to the HPFRCC mixes, a mortar mix was also tested. The mix design for the mortar was identical to the HP-E1 except without the fibers, and is referred to as HP-EM herein. This mortar was studied as a control for identifying the role that the PVA fibers play in resisting tension in ECC at high strain rates.

Mixing was performed in a three-speed tabletop mixer consisting of a vertical rotating paddle. The paddle rotated both around the mixing bowl and on its axis. The entire mixing process lasted approximately 35 min for HP-E1 and over an hour for HP-T1, due to the difficulty in mixing a 2% volume fraction of steel fibers in the tabletop mixer. Cylindrical specimens (Fig. 1) were cast vertically in three lifts with tamping and less than 10 s of vibration at each lift. All specimens remained in their molds for 24 h with the exception of HP-E1A, which remained in the molds for 48 h. After demolding, specimens were wet-cured at room temperature for 15 days and then placed in a 50% relative humidity environment for 12 days until being tested at 28–29 days.

For the study of the effects of specimen geometry on strain capacity, coupon specimens (30.5 cm × 7.6 cm × 1.3 cm) and cylinders (Fig. 1) of HP-E2 were cast from the same batch at the University of Michigan. The cylinders were tested at Stanford University concurrently with the coupons at The University of Michigan at an age of 35 days. To the best of the authors' knowledge, cylindrical specimens have not been previously used for examining the effects of strain rate in HPFRCC materials. It is more common to use coupon specimens or dogbones. Cylindrical specimens in this work were used to stay consistent with previous as well as subsequent work on the rate-sensitivity of these HPFRCC materials in

Table 1 HPFRCC mix proportions by weight

HPFRCC	Portland cement	Silica sand	Class F fly ash	Water	Methyl-cellulose	Super-plasticizer
HP-E1	1.00	0.71	0.43	0.56	0.0027	0.003
HP-E2	1.00	0.80	1.20	0.53	0.0	0.03
HP-T1	1.00	1.00	0.15	0.40	0.0	0.0

Table 2 Properties of fibers used

Fiber material	Diameter (mm)	Length (mm)	Density (g/cm^3)	Tensile strength (MPa)	Modulus of elasticity (GPa)
PVA	0.04	12	1.3	1600	40
Steel	0.3	30	7.9	2470	200

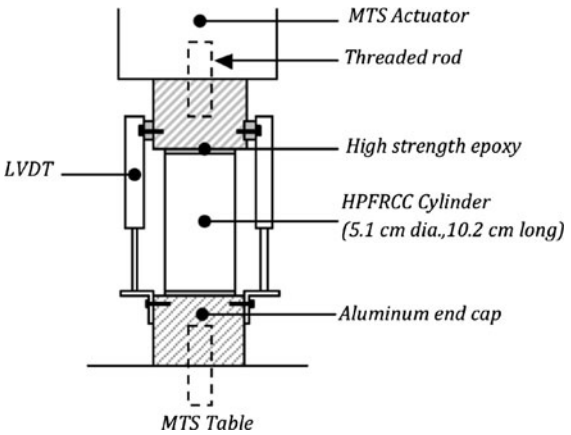

Fig. 1 Test set-up

compression and reversed-cyclic loading [4, 10]. As will be later discussed, the geometry of the tensile specimen chosen significantly affects the tensile response of these materials and is a non-trivial parameter.

3.2 Loading and test-set ups

In general, strain rates in reinforced concrete structures may be as high as 0.05–0.1 s^{-1} during an earthquake [18, 25]. Therefore, to be consistent with these rates, four strain rates were considered for this test series: a quasi-static rate of 2×10^{-5} s^{-1}, a transitional rate of 2×10^{-4} s^{-1}, and "seismic" rates of 0.02 and 0.2 s^{-1}. The two largest strain rates are intended to bracket the rates that the HPFRCC might experience in an earthquake.

For each strain rate, the HPFRCC specimens were subjected to monotonic tension using the setup shown in Fig. 1. Aluminum end caps were attached to the specimens with high strength epoxy and connected to a 250-kN, closed-loop servo-controlled MTS machine with threaded rods, approximating fixed-end boundary conditions (in reality, the actuator has some flexibility and is not rigidly fixed against lateral displacements). Three LVDTs were attached to the end caps to measure the displacement along the full length of the cylinders. Tests were conducted using displacement control, where the control variable was the average displacement of the three LVDTs. The exception to this was the specimens of HP-E1A, in which the displacement of the actuator was used as the control variable. The gage length for these specimens was the entire length of the cylinders, 10.2 cm.

For the study on specimen geometry, the HP-E2 cylinders were tested at Stanford in monotonic tension at a quasi-static strain rate using the test set-up of Fig. 1. The coupon specimens were tested at The University of Michigan under the same loading conditions as the cylinders, but using the test setup described by Li et al. [15].

4 Experimental results

Results from monotonic tension tests of the mortar, HP-E1, and HP-T1 mixes at elevated strain rates are presented here. The phrase *seismic rate* corresponds to the two highest strain rates, and *DIF* stands for dynamic increase factor. *Strain capacity* is defined as the strain at the onset of softening, and the *hardening-phase strength* is the average stress of a line fit through the strain *hardening region*. Additional details are given in Douglas [4].

4.1 Strain rate effect in mortar

The tensile response of the control mortar specimens at various strain rates in terms of peak strength, strain, and stiffness is given in Table 3. Mortar tensile strength increased by 75 and 85%, respectively, from the quasi-static value at the two highest (i.e., seismic) strain rates. These results are consistent with the rate dependence of concrete in tension, which has displayed increases of up to 100% in monotonic tension under similar strain rates [2, 6, 12, 19]. The modulus of elasticity of the mortar increased by 11–17%, although the increase was not consistent with increasing strain

Table 3 Performance of mortar under increasing monotonic tension strain rates

Strain rate (sec^{-1})	Peak strength (MPa)	DIF for peak strength	Strain at peak strength (%)	Modulus of elasticity (GPa)
Quasi-static	1.82	1.00	0.013	14.5
0.0002	2.30	1.26	0.014	17.0
0.02	3.19	1.75	0.021	16.4
0.2	3.36	1.85	0.022	16.1

rate. The magnitude of the increase in tensile modulus agrees with that reported in the literature for the modulus of concrete in tension [12]. It is noted that similar increases in modulus have been reported in compression as well as the trend of the increase in modulus being less significant than the increase in strength with increasing strain rate [3, 25–27, 31, 33].

4.2 Strain rate effect in HP-E1A and HP-E1B

Figure 2 shows the rate dependence of HP-E1A and HP-E1B for a representative sample at each strain rate. Average values for strength and strain capacity of the three specimens tested at each strain rate are presented in Table 4. In addition, the monotonic tension response of all three HP-E1 specimens at the extreme strain rates is presented in Fig. 3, giving an indication of the variability in the test results. In general, specimen-to-specimen variability within each strain rate was relatively low, with a slightly greater variability occurring at the two fastest strain rates. The initial spike in the curves in Fig. 2 is related to the specimen geometry, and represents the formation of the first crack, which in these experiments generally corresponds to the peak tensile strength. By observation, the first crack propagated throughout most of the cross section of the specimen, which is in keeping with Li and Leung's [14] definition of first cracking. The initial spike is further discussed in Sect. 5.1.

There was a consistent increase in first cracking strength with strain rate for both HP-E1A and HP-E1B, with a maximum increase of 81 and 69% at a strain rate of 0.2 s^{-1}, respectively. This increase in first cracking strength is comparable to that of the mortar, which was 75 and 85% for strain rates of 0.02 and 0.2 s^{-1}, respectively. The first cracking strength of the HP-E1 specimens is significantly greater than that of the mortar alone, which has been attributed to fiber bridging once cracking initiates, but prior to the crack propagating through the entire cross-section of the specimen [14].

The trend in the hardening-phase strength (which often occurred at strengths lower than the first crack) was significantly different between the HP-E1 mixes. The hardening-phase strength of HP-E1A increased by 120% when the strain rate was increased from a quasi-static rate to a rate of 0.2 s^{-1}. In contrast,

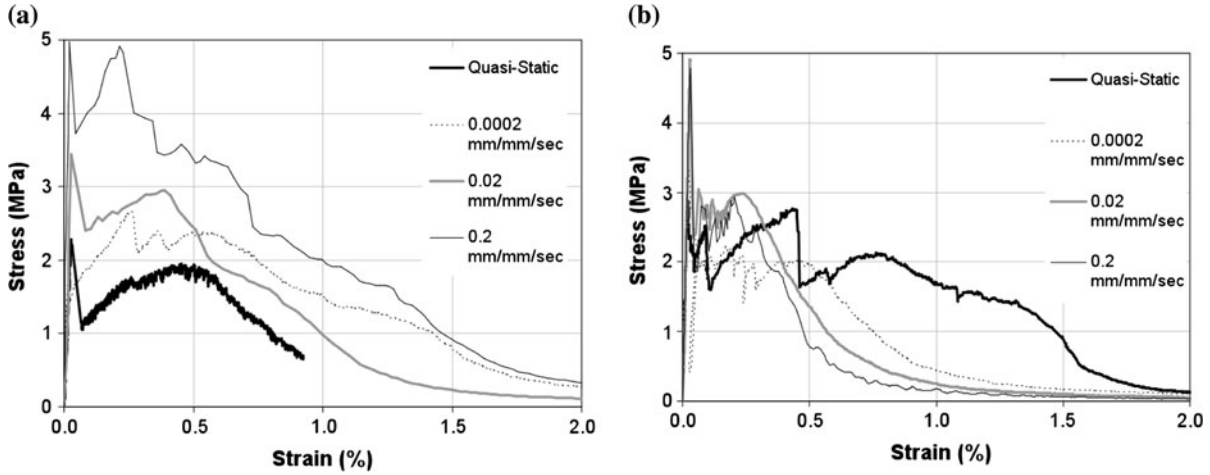

Fig. 2 Rate dependence of **a** HP-E1A and **b** HP-E1B in monotonic tension

Table 4 Average response characteristics of cylindrical HPFRCC material specimens

Strain rate (sec^{-1})	HP-E1A			HP-E1B			HP-T1		
	1st Crack strength (MPa)	Hardening strength (MPa)	Strain capacity (%)	1st Crack strength (MPa)	Hardening strength (MPa)	Strain capacity (%)	1st Crack strength (MPa)	Hardening strength (MPa)	Strain capacity (%)
Quasi-static	2.51	1.73	0.51	2.91	2.30	0.44	2.76	2.08	0.51
0.0002	2.75	2.22	0.56	3.22	2.17	0.51	3.04	2.32	0.29
0.02	3.10	2.27	0.37	4.51	2.88	0.20	4.56	2.51	0.39
0.2	4.55	3.81	0.23	4.91	2.61	0.21	4.98	3.68	0.23

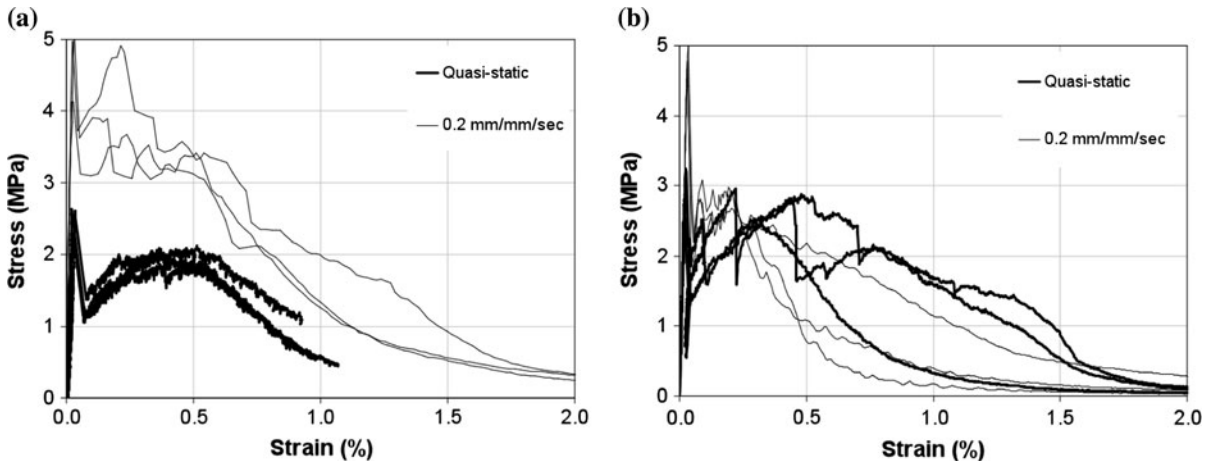

Fig. 3 Monotonic tension response of **a** HP-E1A and **b** HP-E1B at outermost strain rates

HP-E1B exhibited an increase of 25% at a rate of 0.02 s^{-1} and a smaller increase of 13% at a rate of 0.2 s^{-1}. In fact, there was some overlap in the tensile response of the quasi-static and 0.2 s^{-1} specimens for HP-E1B (Fig. 3). The inconsistency between the HP-E1A and HP-E1B specimens with respect to the rate sensitivity of the hardening-phase strength appears to be mostly due to experimental variability. The two sets only differed in the control variable used in the displacement control loading, and HP-E1A cured 24 h longer in the molds before demolding. Neither of these differences is expected to have led to such significant differences in the hardening phase strength. Furthermore, both sets had very similar increases in hardening-phase strength at the lower seismic rate of 0.02 s^{-1}. Therefore, it was only at the upper seismic rate that the rate sensitivity of the two sets deviated from each other. Finally, subsequent experiments on the behavior of identical specimens during reversed cyclic loading [4] have shown strengths in the tension regime at a rate of 0.2 s^{-1} that fall between the strengths of HP-E1A and HP-E1B. Thus, there was a high degree of batch-to-batch variability with respect to the strengths achieved during strain hardening. Note that the ability of the HPFRCC specimens to strain harden will depend on many factors, including matrix toughness and fiber alignment. Fiber alignment (further discussed in Sect. 5.2) is influenced by specimen geometry, casting direction, and casting method, all of which were consistent in the specimens tested here.

The average tensile strain capacity for both sets of HP-E1 specimens decreased by roughly 50% when the strain rate was increased from a quasi-static strain rate to 0.2 s^{-1} (Table 4, Fig. 3). Multiple cracking was observed in the HP-E1 specimens (e.g., Fig. 4) for the quasi-static strain rate, but was essentially not present for the two fastest strain rates (further

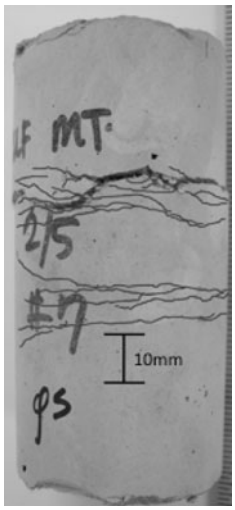

Fig. 4 Cracking in a HP-E1B specimen

discussed in Sect. 5.2). Crack localization and subsequent strain softening occurred where the first crack had formed in all of the specimens, which is not necessarily the case for ECC materials in general.

4.3 Strain rate effect in HP-T1

The rate dependence of HP-T1 is shown in Fig. 5, and average values for the strength and strain capacity at each strain rate are given in Table 4. In many cases, the initial cracking behavior of the HP-T1 specimens differed from that of the HP-E1 mix. The spike at first cracking was less sharp and distinct for HP-T1 than HP-E1 specimens. After the initial strain hardening region post first cracking, the stress decreases sharply and is then typically followed by a second region of strain hardening leading to localization (further discussed in Sect. 5.1).

Both the first-cracking strength and the average hardening-phase strength of the HP-T1 specimens increased monotonically with strain rate. The average hardening-phase strength showed an increase of 77% at the fastest seismic rate of 0.2 s^{-1} relative to the quasi-static rate, and the first cracking strength increased by 165%. The HP-T1 specimens exhibited some residual strength that was not present in the HP-E1 specimens. This residual strength appears to be independent of strain rate, ranging from 0.7 to 1.0 MPa on average at 2% strain, and 0.4 to 0.65 MPa at 3% strain. Similar to HP-E1, increasing the strain rate led to decreases in peak strain capacity of the HP-T1 specimens. When loaded at a rate of 0.2 s^{-1}, the strain capacity decreased by 55% compared to its value at a quasi-static rate. There was very little multiple cracking observed for the HP-T1 specimens (e.g., 2–3 cracks in two locations along the specimen height). Crack localization and strain softening occurred where the first crack formed.

The variability between specimens for the quasi-static and 0.2 s^{-1} strain rate groups can be seen in Fig. 6. HP-T1 specimens generally had a higher variability than HP-E1. The main reason for this higher variability was difficulty in achieving good fiber dispersion at volume fractions above 1%. The fibers had a tendency to interlock and clump together during placement of the mix in the molds, and by observation, some specimens had a larger volume fraction of fibers than others.

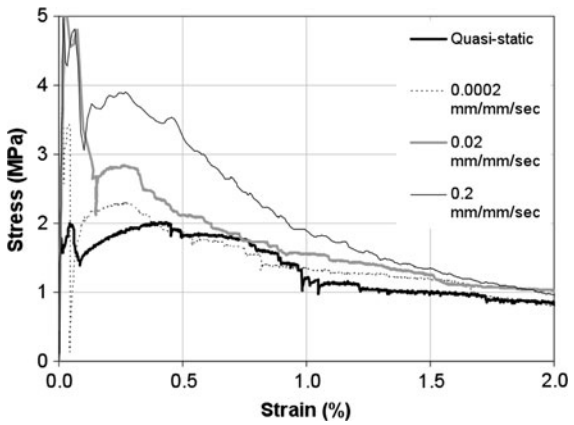

Fig. 5 Rate dependence in monotonic tension of HP-T1 at quasi-static and seismic strain rates

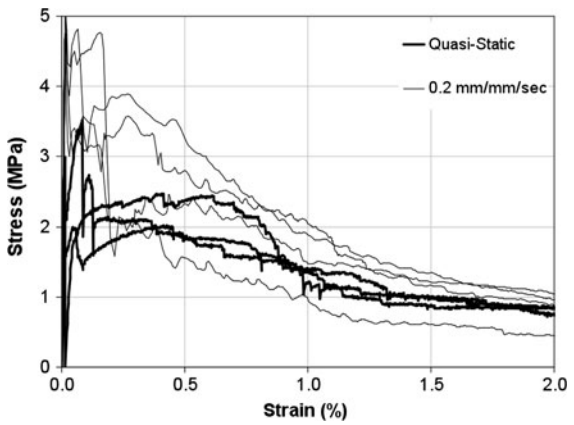

Fig. 6 Monotonic tension response of HP-T1 at outermost strain rates

4.4 Effect of specimen geometry: HP-E2

The monotonic tension response for HP-E2 coupon and cylinder specimens is presented in Fig. 7. Strength and strain capacity values for both specimen types are summarized in Table 5. The first cracking strength for the two specimen types is essentially identical, which would be expected. The strain capacity, however, is over five times greater for the coupon specimens than for the cylinders.

Figure 8 shows the extent of multiple cracking in the cylindrical specimens. It should be noted that the degree of multiple cracking shown in Fig. 9 is among the best observed for the cylindrical specimens. However, it is still much less than the observed multiple cracking in coupon and dogbone specimens (e.g., [11], [16]).

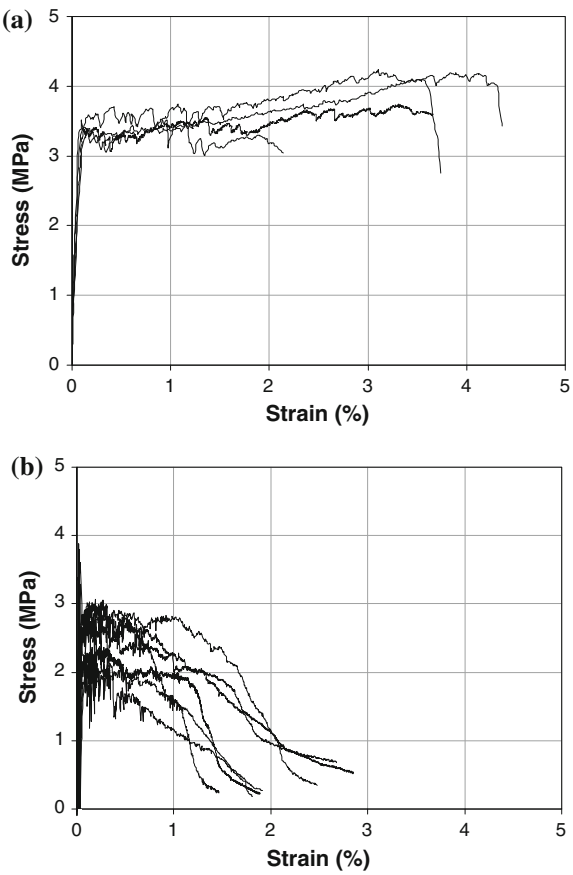

Fig. 7 Monotonic tension response of HP-E2 using **a** coupon specimens and **b** cylindrical specimens (coupon results courtesy of E. Yang and V.C. Li of the University of Michigan)

Table 5 Average quasi-static response characteristics of HP-E2

Geometry	1st Crack strength (MPa)	Hardening strength (MPa)	Strain capacity (%)
Coupon	3.35	3.56	3.35
Cylinder	3.46	2.38	0.63

The strain capacity for the cylinders of HP-E2 was 25–50% greater than for HP-E1, while the hardening phase strength was roughly 40% greater than HP-E1A and essentially equal to HP-E1B. There were two differences between these two mixes: (1) HP-E2 was tested at 35 days as opposed to 28 days for HP-E1, and (2) HP-E2 uses a much higher fly ash content and a much lower w/cm ratio (Table 1). It is expected that the slight change in the age at testing will be much less significant than the effects due to mix design. As discussed in Wang and Li [32], a low w/cm ratio facilitates fiber distribution, while a high fly ash content reduces the interfacial bond of the fibers and the matrix toughness, both of which improve potential strain hardening and multiple cracking.

5 Further discussion and analysis of results

5.1 Stress–strain response characteristics and multiple cracking

In the HP-T1 specimens, two strain hardening regions, at different strengths, were typically observed (e.g., Fig. 5). The second, lower strength, strain hardening region is attributed to a redistribution of stress from fibers aligned more in the direction of loading that have fractured or pulled out, to fibers aligned at an angle relative to the direction of loading. Fibers aligned at an angle are less efficient in resisting stress and therefore have a lower fiber bridging stress. However, the stiff, steel fibers at an angle provide some shear resistance, allowing for a second, lower strength, level of strain hardening.

For the HP-E1 and HP-E2 mix designs (i.e., ECC), a stress–strain response similar to that in Fig. 9 was observed. In this case there is no strain hardening to loads above the first cracking strength (as there was observed in the HP-T1 specimens) but rather a drop in strength and a single, lower-than-cracking-strength

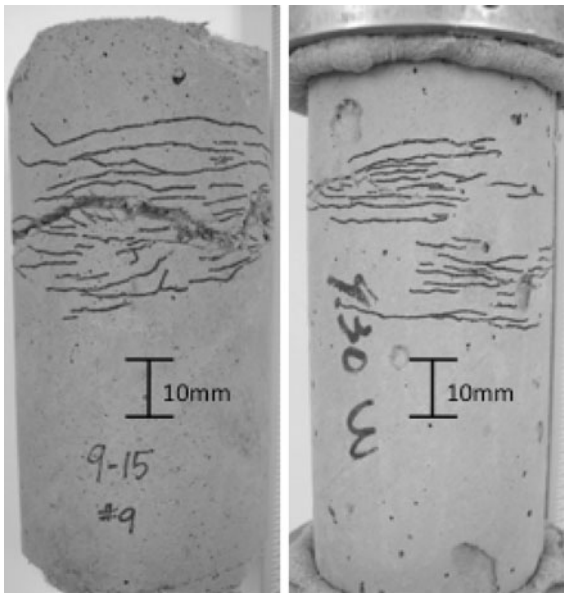

Fig. 8 Multiple cracking of cylindrical HP-E2 specimens

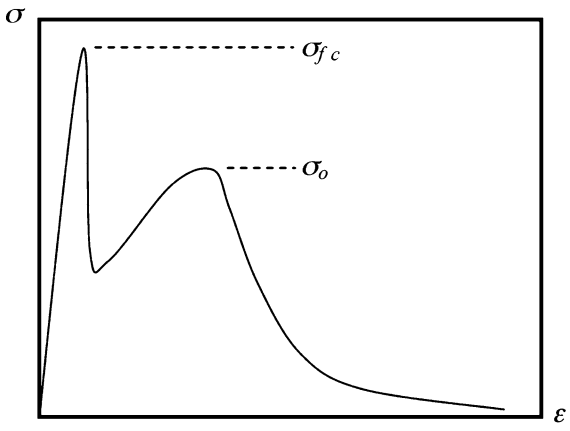

Fig. 9 Expected stress–strain response of ECC with a first crack strength, σ_{fc}, greater than the maximum bridging strength, σ_0 (adapted from Li and Leung [14]

strain-hardening region. This response represents the response of ECC when the internal flaw size is small (which applies to the fine mortar matrix of HP-E1 and HP-E2) and the first cracking strength is greater than the maximum bridging stress of the fibers. As a result, the fibers are not able to sustain the load shed by the matrix after the first crack forms. In this case the strength criterion for multiple cracking and associated strain hardening to occur is not met (criterion are summarized in Li [13]) and the fibers will completely pull out or fracture. Evidence of both fiber fracture and pull-out were observed (see Sect. 5.2). Strain hardening and the associated strain capacity of the material was therefore hindered.

There are two possible causes identified for this stress–strain behavior in the HP-E1 and HP-E2 specimens studied here that, unlike the causes reviewed above, are material (constituent) independent. They are: (1) specimen geometry (and casting direction), and (2) testing boundary conditions. Comparing the results from coupon (Fig. 8a) and cylinder (Fig. 8b) specimens from the same batch of material, HP-E2, the coupon specimens had five times the strain capacity, and a smoother transition from first cracking to strain hardening (i.e., there is no spike in the stress–strain response at first cracking as diagrammed in Fig. 9). Furthermore, the coupon specimens had a higher degree of multiple cracking. The coupon and cylinder specimens of HP-E2 were both made from the same batch of ECC, both tested in approximately fixed–fixed conditions, and both tested at the same strain rate, implying that specimen geometry is likely responsible for the significantly different tensile response between the cylinder and coupon specimens. Cylindrical specimens allow for a random, three-dimensional nature of fiber alignment. Such alignment leads to less efficient fiber bridging than an alignment more predominantly oriented in the direction of loading (as also suggested by Kanakubo et al. [8]) and likely lowers the maximum fiber bridging stress to a value below the first cracking strength, giving a response similar to that in Fig. 9. In thin coupon specimens, more fibers are aligned in the direction of loading, and therefore the fiber-bridging stress is adequate to promote multiple cracking without the large drop in stress after first-cracking. Differences in cylinder and coupon specimen response have also been observed and reported by others [8, 10]. The response described in Fig. 9 was observed in the cylinders at all strain rates herein.

Testing boundary conditions could also play a role in the stress–strain response. In Kesner et al. [10], cylindrical specimens tested in a pin-fixed configuration showed a drop in stress at first cracking that was roughly 20–30% of the first crack strength. These specimens showed more multiple cracking than the results presented here and they also had an ultimate stress in all cases but one that exceeded the first cracking strength. It is possible that the pin connection helped alleviate secondary moments that are

typical in tension tests using fixed–fixed boundaries, which lead to a slight increase in tensile strength and higher fracture energy [29, 30]. However, Kanakubo et al. [8] report results of two sets of cylinders, one with pin-fixed end conditions and the second with fixed–fixed end conditions. For the pin-fixed set, a 25–35% drop in stress was observed followed by minimal strain hardening and the fixed–fixed specimens exhibited a smaller drop in stress after first cracking. More research is needed to understand the impact of boundary conditions and geometry on the uniaxial tensile stress versus strain response of HPFRCC materials.

Finally, it should be noted that the absence of multiple cracking has an impact on the interpretation of "strain" in the stress–strain curves presented in this work. For thinner HPFRCC specimens, which experience considerable multiple cracking, the calculated strain across the gage length acts as a more realistic material strain (i.e., the strain is independent of the gage length chosen). For the cylindrical specimens in this work that experienced very moderate multiple cracking, the strain, calculated as the deformation of the cylinder divided by the cylinder length is dependent on gage length. This method of quantifying the deformation of the cylinders using LVDTs over the entire cylinder length was chosen to be consistent with subsequent measurements in the compression and reversed cyclic tests at elevated strain rates [4].

5.2 Fiber behavior

As discussed previously, strain hardening and multiple cracking of HPFRCC materials are accompanied by fiber pullout, which also includes untwisting in the case of the steel fiber mix. To verify the presence of fiber pullout in this research, scanning electron microscope images were taken of the failure planes for the cylindrical specimens of HP-E1B, HP-E2, and HP-T1. Monotonic tension specimens from both the quasi-static and 0.2 s^{-1} seismic rate tests were observed for the HP-E1B and HP-T1 mixes. The same mechanisms were observed for the specimens at each of the strain rates, and only photos for the quasi-static specimens are presented here. For HP-E2 specimens, only quasi-static specimens were tested and observed.

The fracture surface of an HP-T1 specimen is shown in Figs. 10 and 11 and indicates that a variety of mechanisms occurred during specimen cracking. Pullout channels and intact fiber ends in Fig. 10 provide evidence of fiber pullout, while fractured fibers with their sharp, angled failure planes can be seen in Fig. 11a. These angled failure planes likely formed as a result of the combination of untwisting and direct tension acting on the fibers during pullout. The untwisting action of the fibers during pullout straightens the initially helical fibers, as shown in Fig. 11b. Note the gap between the fiber and the matrix as well as radial cracking around the fiber in Fig. 11b, indicating debonding and pullout for this fiber. Again, similar response was seen in the higher strain rate specimens viewed.

The fracture surface of HP-E1B and HP-E2 specimens is shown in Figs. 12 and 13, respectively. In general, the HP-E1B specimens exhibited a mix of fiber pullout and fracture (Fig. 12a) and the HP-E2 cylindrical specimens showed both pullout (Fig. 13) and delamination (Fig. 12b) behavior. Fiber fracture limits the potential strain capacity of the material, which is reflected in the lower strain capacity of HP-E1B compared with cylinders from HP-E2. The delamination of the outer layers of the PVA fibers in Fig. 12b is caused by abrasion from the matrix during pullout and has been observed in cases where the PVA fibers have a high chemical and frictional bond with the matrix [13]. In contrast to the fractures observed for HP-E1B, Fig. 13a shows channels on the surface of HP-E2 specimens where fibers have pulled out of the matrix. Intact fibers for HP-E2 after pullout can be seen in Fig. 13b.

Although pullout and fracture were observed for HP-E1B at both quasi-static and seismic strain rates through the SEM images, it is believed that fracture was more prevalent at the seismic rates due to increased toughness of the matrix with strain rate as seen in the measured stress–strain response of the mortar, and increased chemical bond strength between the fiber and matrix at high strain rates [34].

5.3 Response relative to previously reported research

In this work, the first cracking strength of HP-E1 increased by 81 and 69% for the A and B sets, and the hardening-phase strength increased by 120 and 25%

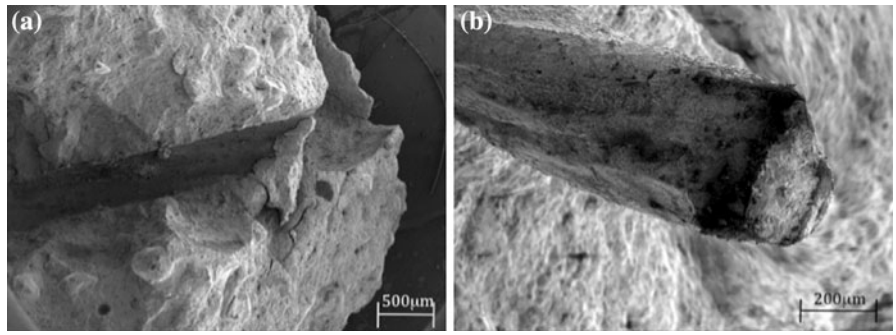

Fig. 10 **a** Pullout channel and **b** intact fiber end after pullout in HP-T1 specimens

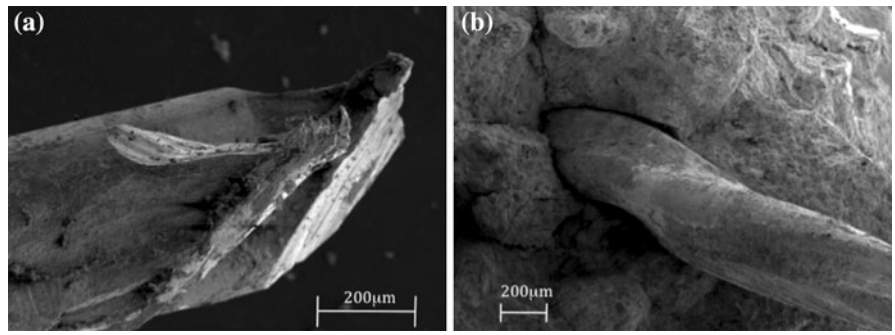

Fig. 11 **a** Fiber fracture, and **b** untwisting of the helical fibers in HP-T1 specimens

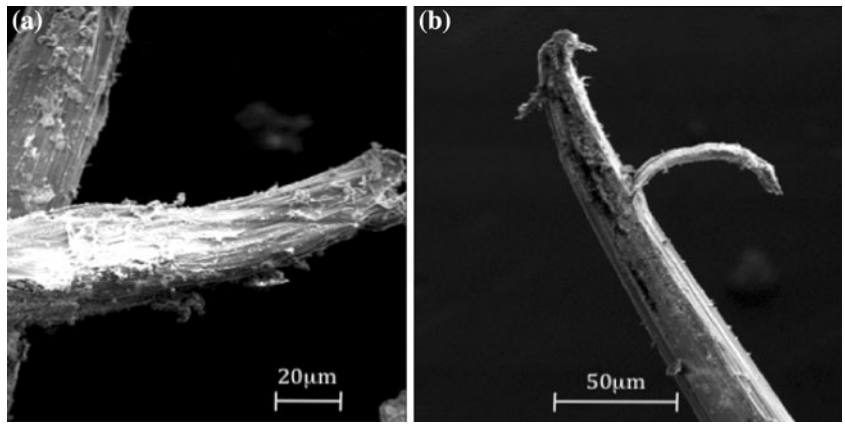

Fig. 12 **a** Fiber fracture and delamination in an HP-E1B specimen and **b** fiber delamination observed in an HP-E2 specimen

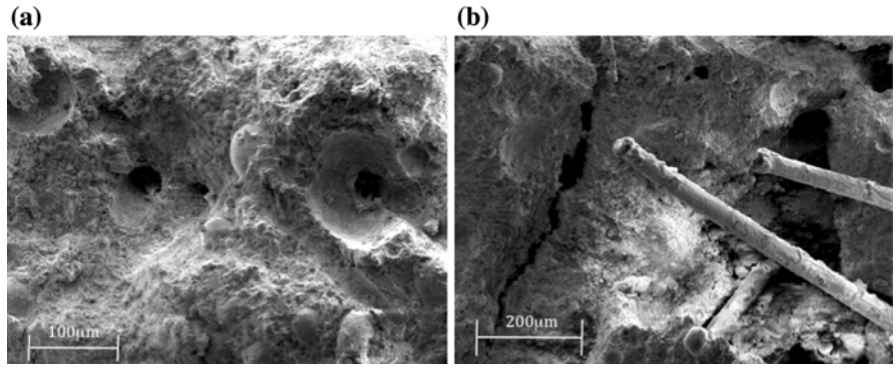

Fig. 13 Evidence of pullout with **a** channels and **b** in tact fibers in HP-E2 specimens

for the A and B sets, respectively, at seismic strain rates. The corresponding strain capacity decreased by 50% for both sets of HP-E1. Yang and Li [34] reported a strength enhancement of 150% and a strain capacity reduction of 80% in thin coupon specimens, while Maalej et al. [17] showed strength enhancements of 100% and no change in ductility due the lack of chemical bond between the polyethylene fibers and cement matrix, also in thin coupon specimens. Given the nature of the fiber alignment of the thin coupon specimens, the rate sensitivity of strength and strain capacity is expected to be greater than in specimens with less efficient fiber bridging, such as cylindrical specimens of HP-E1, as is confirmed here.

For the steel fiber HP-T1 specimens, the first cracking strength increased by 165%, hardening-phase strength increased by 77%, and strain capacity decreased by 50% at the seismic strain rates. Kim et al. [11] reported increases with strain rate in first cracking strength and post-cracking strength up to 100 and 73%, respectively, depending on matrix strength and fiber volume fraction. The high strength of the composite at higher strain rates was hypothesized to be from fiber fracture occurring rather than pulling out. From the SEM images observed by the authors, it was found that indeed some fibers fractured, and pullout (untwisting with radial and longitudinal cracking) was also observed. Kim et al. observed more multiple cracking at all strain rates than were observed here, and it is proposed that this is due to specimen geometry. Kim et al.'s specimens were dogbone-shaped with a 25 mm cross section, cast horizontally, and so a tendency for fiber alignment in the direction of loading would be expected. While a consistent decrease in strain capacity was observed here in the cylindrical specimens, Kim et al. found no clear trends for strain capacity, which showed decreases of up to 40% and in some cases increases of up to 32% at higher strain rates.

6 Implications for seismic applications

The effect of strain rate on the ductility of HPFRCC materials as observed in this study may impact the structural performance of reinforced HPFRCC elements. As an example, cyclic lateral load tests on reinforced HPFRCC infill panels (using a mix similar to HP-E1) for seismic retrofitting of steel-framed buildings have demonstrated that the structural strength of these panels can increase as much as 35% relative to similarly reinforced panels made of traditional concrete [9]. Similar results have been found with steel fiber HPFRCC materials similar to HP-T1 [23]. The increase in structural strength was attributed to the tensile, and therefore, shear capacity and ductility of the HPFRCC material. At increasing drift levels, the HPFRCC panels maintained their integrity, leading to a higher structural strength and more hysteretic energy dissipation than the reinforced concrete panel. Consequently, decreases in the ductility of the HPFRCC with increased strain rate may limit the potential increase in strength and hysteretic energy dissipation possible in applications that combine HPFRCC and steel reinforcement.

7 Conclusions

Two HPFRCC materials were tested in monotonic tension at strain rates ranging from quasi-static to seismic-level ($0.2\ s^{-1}$). One material was an ECC (HP-E specimens) and the other a twisted, high strength steel fiber HPFRCC (HP-T specimens). Cylindrical specimens were used to represent bulk properties in structures and to be consistent with subsequent work on the cyclic (tension–compression) and compressive strength response of these materials at varying strain rates [4]. The effects of specimen geometry on the monotonic tension response of one of the HPFRCC materials, ECC, was also examined by comparing the behavior of cylindrical and coupon specimens cast from a single batch of material.

Both tensile strength and strain capacity of the HPFRCC materials are significantly affected by increasing strain rate. For HP-E1 mixes, the strength increased from 25 to 120% when moving from quasi-static to seismic strain rates, while the HP-T1 mix experienced strength enhancement ranging from 77 to 165%. Strength enhancement for both mixes was evaluated in terms of first cracking strength only and the average strength over the strain-hardening region (referred to as hardening-phase strength in this work). Generally, the first cracking strength exhibited a greater and more consistent increase in strength than the hardening-phase strength with increasing strain rates. Both HPFRCC materials studied here

experienced a 50–55% decrease in strain capacity when strain rate was increased to seismic levels. Little multiple cracking was observed for the cylindrical specimens during quasi-static loading, with crack localization often occurring at the location of first cracking. At seismic rates, no multiple cracking was observed.

SEM images taken of the fracture plane of the specimens indicate that pullout and fracture of the fibers occurred for both HPFRCC mixes. In general, fiber fracture was more prevalent for HP-E1 than for HP-E2 and was reflected in the lower strain capacity of HP-E1. The prevalence of fiber pullout in the HP-E2 specimens is likely due to the higher fly ash content and lower w/cm ratio of HP-E2, both of which have been shown to be favorable to strain hardening and fiber dispersion [32]. Both fiber pullout, fiber untwisting, and radial cracking around the fibers were observed in the HP-T1 mixes.

Due to the low multiple cracking and low tensile strain capacity of the materials under quasi-static loading, an additional geometry study for an ECC mix was conducted in collaboration with researchers at The University of Michigan at Ann Arbor. Coupon specimens were observed to have over five times the strain capacity of cylindrical specimens made from the same batch of material. A sharp decrease in stress after first cracking and limited strain hardening was also observed for the cylindrical specimens and was not observed in the coupon specimens.

For the ECC mixes, it is believed that the lack of multiple cracking, the sharp decrease in stress after first cracking, and the limited strain-hardening observed in the cylindrical specimens (at all strain rates) is due to the random, three-dimensional nature of the fiber alignment in cylinders as well as the vertical casting direction. The random fiber alignment leads to fewer fibers aligned in the direction of loading, producing less efficient fiber bridging, and therefore lowering the maximum fiber bridging stress to a value below the first cracking strength. For the high strength, twisted steel fiber mix, the limited multiple cracking and strain-hardening response is attributed to vertical casting as well as the difficulties of casting the mix into a relatively small mold. As with the ECC mixes, there was a tendency for the steel fibers to be oriented perpendicular to the loading direction when cast vertically. Furthermore, clumping of the fibers resulted in variable fiber contents in the specimens, as evidenced by the higher variability in the HP-T1 results.

Results from this research can be used to estimate the impact of loading rates on the global response of structures using HPFRCC materials through rate-dependent constitutive models. In addition, information from these experiments can shed light on material-level response to allow for new HPFRCC mix designs to be engineered for improved performance under strain rates experienced during seismic loading. The research further illustrates the importance of specimen geometry to the observed tensile behavior of HPFRCC materials and the need for test methods that provide a more robust measure of response that can be used to accurately predict structural performance. Ongoing work by the second author is evaluating the response of HPFRCC mixes in large-scale dogbone specimens to limit the fiber orientation issues present in small geometries with specific casting directions. For the high strength, twisted steel fiber mixes, a larger cylindrical shape should be used to represent bulk material properties and ensure better fiber distribution than was achieved in this research.

Acknowledgments The authors would like to thank Prof. Antoine Naaman for his valuable input at the outset of this research. The authors gratefully acknowledge En-Hua Yang and Prof. Victor C. Li for their contributions in producing the coupon and cylindrical specimens of HP-E2, and testing the coupon specimens of HP-E2, reported in Fig. 7a of this paper. Their efforts and collaboration are greatly appreciated.

References

1. Billington SL (2004) Damage-tolerant cement-based materials for performance-based earthquake engineering design: research needs. In: Li VC et al (eds) Fracture mechanics of concrete structures. Aedificatio Publishers, Freiburg, Germany, pp 53–60
2. Cowell WL (1966) Dynamic properties of plain Portland cement concrete. Technical report no. R447, U.S. Naval Civil Engineering Lab., Port Hueneme, CA
3. Dilger WH, Koch R, Kowalczyk R (1984) Ductility of plain and confined concrete under different strain rates. J Am Concr Inst 81(1):73–81
4. Douglas KS (2007) Rate-dependence in high performance fiber-reinforced cementitious composites for seismic retrofits. PhD Thesis, Stanford University, Stanford, CA
5. Douglas KS, Billington SL (2005) Rate dependence in high-performance fiber-reinforced cement-based composites for seismic applications. Proceedings of the 5th international conference on construction materials, ConMat05, Vancouver, BC, August

6. Fu HC, Erki MA, Seckin M (1991) Review of effects of loading rate on reinforced concrete. J Struct Eng 117(12): 3660–3679
7. Han TS, Feenstra PH, Billington SL (2003) Simulation of highly ductile fiber-reinforced cement-based composites under cyclic loading. ACI Struct J 100(6):749–757
8. Kanakubo T, Shimizu K, Katagiri M, Kanda T, Fukuyama H, Rokugo K (2005) Tensile characteristics evaluation of DFRCC—round Robin test results by JCI-TC. In: Li VC, Fischer G (eds) Proceedings of the international workshop on high performance fiber reinforced cementitious composites in structural applications, Honolulu, Hawaii, USA, 23–26 May 2005
9. Kesner KE, Billington SL (2005) Investigation of infill panels made from engineered cementitious composites for seismic strengthening and retrofit. ASCE J Struct Eng 131(11):1712–1720
10. Kesner KE, Billington SL, Douglas KS (2003) Cyclic response of highly ductile cement-based composites. ACI Mater J 100(5):381–390
11. Kim DJ, El-Tawil S, Naaman AE (2009) Rate-dependent tensile behavior of high performance fiber reinforced cementitious composites. Mater Struct 42:399–414
12. Komlos K (1969) Factors affecting the stress-strain relation of concrete in uniaxial tension. J Am Concr Inst 66(2): 111–114
13. Li VC (2003) On engineered cementitious composites (ECC): a review of the material and its applications. J Adv Concr Technol 1(3):215–230
14. Li VC, Leung C (1992) Steady-state and multiple cracking of short random fiber composites. J Eng Mech 118(11): 2246–2264
15. Li VC, Mishra DK, Wu HC (1995) Matrix design for Pseudo strain-hardening fiber reinforced cementitious composites. RILEM J Mater Struct 28(183):586–595
16. Li VC, Wang S, Wu C (2001) Tensile Strain-hardening Behavior of PVA-ECC. ACI Mater J 98(6):483–492
17. Maalej M, Quek ST, Zhang J (2005) Behavior of hybrid-fiber engineered cementitious composites subjected to dynamic tensile loading and projectile impact. J Mater Civil Eng 17(2):143–152
18. Mahin SA, Bertero VV (1972) Rate of loading effects on uncracked and repaired reinforced concrete members. Report No. UBC/EERC-72/9, Earthquake Engineering Research Center, University of California, Berkeley
19. Malvar LJ, Ross CA (1998) Review of strain rate effects for concrete in tension. ACI Mater J 95(6):735–739
20. Naaman AE (2003) Engineered steel fibers with optimal properties for reinforcement of cement composites. J Adv Concr Technol 1(3):241–252
21. Naaman AE (2003b). Strain hardening and deflection hardening fiber reinforced cement composites. In: Naaman AE, Reinhardt HW (eds) Fourth international workshop on high performance fiber reinforced cement composites (HPFRCC4), Ann Arbor, USA. RILEM Publications, France, June, pp 95–113
22. Naaman AE, Reinhardt HW (2003) Preface. In: Naaman AE, Reinhardt HW (eds) Fourth international workshop on high performance fiber reinforced cement composites (HPFRCC4), Ann Arbor, USA. RILEM Publications, France, June, pp XI–XII
23. Olsen EC, Billington SL (2009) Evaluation of precast, high-performance fiber-reinforced concrete infill panels for seismic retrofit of steel frame buildings: phase 1—cyclic testing of single panel components. Technical report no. 158, John E. Blume Center for Earthquake Engineering, Stanford University, January
24. Parra-Montesinos G (2003) HPFRCC in earthquake-resistant structures: current knowledge and future trends. In: Naaman AE, Reinhardt HW (eds) High performance fiber-reinforced cement composites, proceedings of the 4th international RILEM Workshop, Ann Arbor, MI. RILEM Publications S.A.R.L., France, pp 453–472
25. Scott BD, Park R, Priestly MJN (1982) Stress-strain behavior of concrete confined by overlapping hoops at low and high strain rates. J Am Concr Inst 79(1):13–27
26. Soroushian P, Choi K-B, Alhamad A (1986) Dynamic constitutive behavior of concrete. J Am Concr Inst 83(2): 251–259
27. Sparks PR, Menzies JB (1973) The effect of rate of loading upon the static and fatigue strengths of plain concrete in compression. Mag Concr Res 25(83):73–80
28. Sujivorakul C, Naaman AE (2003) Modeling bond components of deformed steel fibers in FRC composites. In: Naaman AE, Reinhardt HW (eds) Fourth international workshop on high performance fiber reinforced cement composites (HPFRCC4), Ann Arbor, USA. RILEM Publications, France, June, pp 35–48
29. van Mier JGM, van Vliet MRA (2002) Uniaxial tension test for the determination of fracture parameters of concrete: state of the art. Eng Fract Mech 69:235–247
30. van Mier JGM, Vervuurt A, Schlangen E (1994) Boundary and size effects in uniaxial tension tests: a numerical and experimental study. In: Bažant ZP (ed) Fracture and damage in quasibrittle structures: experiment, modelling and computer analysis: proceedings of the US-Europe workshop on fracture and damage in quasibrittle structures, Prague, Czech Republic, 21–23 September 1994, pp 289–s302
31. Wakabayashi M, Nakamura T, Yoshida N, Iwai S, Watanabe Y (1980) Dynamic loading effects on the structural performance of concrete and steel materials and beams. In: Proceedings of the seventh world conference on earthquake engineering, vol 6, part 3, Istanbul, Turkey, pp 271–278
32. Wang S, Li VC (2005) Polyvinyl alcohol fiber reinforced engineered cementitious composites: material design and performances. In: international workshop on HPFRCC in structural applications, 23–26 May Honolulu, HI, USA
33. Watstein D (1953) Effect of straining rate on the compressive strength and elastic properties of concrete. J Am Concr Inst 49(8):729–744
34. Yang E, Li VC (2005) Rate dependencies in engineered cementitious composites. In: International workshop on HPFRCC in structural applications, May 23–26, Honolulu, HI, USA